

*Full Length Research Paper*

# Preparation of thermal neutron absorber based $B_4C/TiO_2$ /polyaniline nanocomposite

Seyed Hossein Hosseini<sup>1\*</sup>, Mona Tarakameh<sup>2</sup> and Sama S. Hosseini<sup>3</sup>

<sup>1</sup>Department of Chemistry, Faculty of Science, Islamshahr Branch, Islamic Azad University, Tehran, Iran.

<sup>2</sup>Department of Applied Chemistry, Faculty of Pharmaceutical Chemistry, Pharmaceutical Sciences Branch, Islamic Azad University, Tehran, Iran.

<sup>3</sup>Department of Veterinary, Faculty of Veterinary, Science and Research Branch, Islamic Azad University, Tehran-Iran

Received 15 November, 2019; Accepted 12 February, 2020

**B<sub>4</sub>C nanoparticles (NPs) have been integrated at that point veiled by TiO<sub>2</sub> NPs lastly composited by utilizing polyaniline (PANI), (B<sub>4</sub>C/TiO<sub>2</sub>/PANI). Shields of thermal neutrons by B<sub>4</sub>C/TiO<sub>2</sub>/PANI have been considered, B<sub>4</sub>C/TiO<sub>2</sub>/PANI nanocomposite was described by FTIR spectroscopy, and nanometer size, morphology, and structures of tests were estimated by SEM and XRD. The electric property was additionally performed by the four-test system. The thermal neutron ingestion of nanocomposites was researched at 0.025 eV. The lessening coefficients of neutrons of B<sub>4</sub>C/TiO<sub>2</sub>/PANI with various thicknesses were estimated, without advantageous materials. The straight lessening coefficients, level of ingestion and half-esteem thickness (HVT) have been estimated and determined by means of full width at half most extreme (FWHM).**

**Key words:** B<sub>4</sub>C nanoparticles, polyaniline, nanocomposite, thermal neutron absorber.

## INTRODUCTION

Neutrons are created by atomic reactors and molecule quickening agents. A thick layer of plastic or water eases back neutrons. For ingestion of ionizing radiation, distinctive metal materials are utilized, for example, lead (Azooz and El-Batat, 2009), earthenware production (Celli et al., 2006), cadmium (D'Mellow et al., 2007), boron (Zhang et al., 2013), and Zirconium (Onimus et al., 2013). In any case, the issue of making or moving the thick defensive layers exists and is hard to fix as it can't meet the advancement needs of the atomic force industry. In this way, the polymeric composites loaded up with metal absorbers have the benefit of being

advantageous and safe in the atomic condition, which is turning into the focal point of the atomic insurance inquire about (Bartali et al., 2009). Polymeric mixes can assist us with expanding the protecting property particularly low vitality radiation (Nambiar and Yeow, 2012; Kim and Cho, 2019). Conductive polymers by having conjugated twofold bonds have significant jobs in making the electric flow, and in the retention of electromagnetic waves are likewise extremely compelling. As of late, ferromagnetic and ferroelectric-leading polymer composites have gotten significant consideration, particularly in investigations of composite materials with various kinds of ferromagnetic

\*Corresponding author. Email: [dr.shhosseini@gmail.com](mailto:dr.shhosseini@gmail.com).

or ferroelectric fillers (Hosseini et al., 2015a; Hu et al., 2018; Chen et al., 2019).

In recent years, broad studies have been led on the assurance of atomic pillars, for example, neutrons and gamma beams. The greater part of these adsorbents depends on lead or boron or their subsidiaries like B4C. These mixes are utilized as a composite with mechanical polymers, for example, polyethylene, polypropylene or polystyrene. Be that as it may, the polyethylene plastic plates as a defensive material additionally have their inadequacies of applied temperature by about 100°C, which can just meet the prerequisites at room temperature. For applying at a higher temperature, for example, an atomic reactor, particularly the occasion of radiation mishaps, the polyethylene plastic plates may get liquefied and lose their defensive capacity (Wozniak et al., 2017).

Sukegawa et al. (2011) detailed a delicate kind neutron-protecting sap that has been created by improving a current hard-type neutron protecting material utilizing the epoxy-based tar as extra protecting material. An adaptable warmth safe neutron-protecting material has been created, which is comprised of another polymer-based gum with boron. A recently adaptable warmth safe neutron-protecting tar has been created. A "Sandwich" kind of neutron protecting composite strengthened via carbon fiber was presently concentrated by Yiping et al. (2013). For protecting plan, neutrons and  $\gamma$ -beams (or X-beam) are the fundamental sorts of atomic radiation, which ought to be considered, since any shield that constricts neutrons and  $\gamma$  - beams will be increasingly viable for weakening different radiations. Therefore, a study of the impact of these beneficial cementation materials, on the gamma and neutron protecting properties of solid materials is possibly helpful in the improvement of the utilization of such materials in protecting plan (Fugaru et al., 2015).

In the first works, we have incorporated a few papers of microwave retaining materials (Hosseini et al., 2015b, 2016) and X-beam (Hosseini et al., 2015c; Hosseini and Soltanabadi, 2016) lessening dependent on directing polymers and nanoparticles. Then again, various absorbers in the various areas have been readied (Hosseini and Zamani, 2016; Dolabi et al., 2019; Hosseini et al., 2019). Right now, weakening coefficients of neutrons of B4C/TiO<sub>2</sub>/PANI with various thicknesses were estimated, without advantageous materials, at the vitality of 0.025 eV. At that point test esteems were utilized to gauge some cooperation parameters, for example, direct constriction coefficients and half-esteem thicknesses. The point of the present work is the figuring of straight lessening coefficients and half-esteem thicknesses for another class of absorbers utilizing directing polymer composites based conductivity and

nuclear thickness.

## METHODOLOGY

### Materials

Refined and deionized water was utilized all through the work. Boric corrosive was gotten from Merck and was refined by taking shape from warm water. Polyvinyl liquor was gotten from Aldrich and is utilized as it is gotten. Aniline monomer (explanatory evaluation, Merck) was refined twice under decreased tension and put away underneath 0°C. TiO<sub>2</sub> particles and dodecylbenzene sulfonic corrosive (DBSA), smelling salts persulfate (APS), and alkali (NH<sub>3</sub>) were bought from Merck. Different synthetic compounds were of explanatory evaluation and utilized moving along without any more filtration.

### Preparation of B4C

26.4 g (0.6 mol) of polyvinylalcohol (PVA) was made dissolvable in refined water taken in a 500 ml measuring utensil and warmed on a water-shower. 12.366 g (0.2 mol) of boric corrosive B(OH)<sub>3</sub> was made dissolvable in refined water taken in a 250-ml container and warmed in the water shower. At that point, the boric corrosive arrangement was added to the PVA arrangement in hot conditions with steady mixing with a glass bar. A white floppy and rubbery material were acquired which was gathered and dried in a broiler at about 100°C. From there on, the dry material was ground to white powder. The polymer was put in a porcelain cauldron and warmed in a heater. A warming pace of 120°C every hour was kept up till the ideal temperature was come to. Pyrolysis of the antecedent compound noticeable all around for three hours yields a dark powder at the two temperatures (400 and 800°C) (Modal and Banthia, 2005).

### Preparation of PANI

PANI was set up by the ordinary polymerization strategy, within the sight of APS as oxidant and DBSA as the surfactant and dopant. Dopant was broken up in refined water with lively blending for around 30 min under mixing for around 1 h. Aniline monomer was included and mixed for 30 min. APS (equivalent to a molar proportion of aniline) was broken down in 30 mL deionized water and was gradually included drop-wise under consistent blending. Polymerization was permitted to continue at 0-5°C for 4 h. PANI was acquired from green-dark powder by sifting and washing the suspension with deionized water and ethanol, separately. PANI was dried under a vacuum stove at 40°C for 12 h. Moreover, unadulterated PANI was set up as per the union depicted above, under a similar condition except if there were no dopants left during the technique. Undoped PANI was set up by ordinary response technique subsequent to mixing doped PANI under NH<sub>3</sub> (2M) answer for 24 h.

### Preparation of TiO<sub>2</sub> masked B4C

To expand the extremity of the adsorbent and to encourage its uniform dispersion inside the composite, we covered B4C with TiO<sub>2</sub>. 0.1 g of TiO<sub>2</sub> NPs and diverse weight proportions of B4C in 100 ml of completely scattered water, balanced the arrangement pH to 6 and were oppressed under ultrasonic light for 5 min. Under these conditions, the B4C surface is decidedly charged and the TiO<sub>2</sub> surface contrarily charged. At the point when the two arrangements are blended in with ultrasonic radiation, the TiO<sub>2</sub> nanoparticles are very much covered on B4C. The subsequent

blend is separated and dried at room temperature. What's more, these items can be set up by mechanical and physical blending following one hour by pivoting the blender.

### Synthesis of B<sub>4</sub>C/TiO<sub>2</sub>/PANI nanocomposites

B<sub>4</sub>C/TiO<sub>2</sub>/PANI as center shell nanocomposite was set up by in situ polymerizations within the sight of DBSA as the surfactant and dopant and APS as the oxidant. The 0.1 g DBSA was broken up in

refined water with overwhelming mixing for around 20 min. The B<sub>4</sub>C/TiO<sub>2</sub> nanoparticles were added to the DBSA arrangement under the blending conditions for around 1 h. At that point, 1 mL of naturally refined aniline as monomer was added to the suspension and mixed for 30 min. The B<sub>4</sub>C/TiO<sub>2</sub> nanoparticles were scattered well in the blend of aniline/DBSA under ultrasonication for 2 h. 3.28 g APS as initiator was broken up in 60 mL 0.1 M HCl and added drop-wise to the mixed response blend. Polymerization was permitted to continue while blending in an ice-water shower for 4 h. The nanocomposite was gotten by separating and washing the suspension with deionized water and ethanol, individually. The acquired dark-colored green powder containing (with various weight proportion, 20, 50 and 80wt% B<sub>4</sub>C) B<sub>4</sub>C/TiO<sub>2</sub>/PANI was dried under vacuum for 24 h.

### Sample preparation

In order to evaluate neutron attenuation properties, all the sample disks form were fabricated by molding under a hydraulic press at 10 MPa pressure at room temperature for a few minutes. Following this procedure, samples with 1 cm radius and various thicknesses between 1-2 mm were produced.

### Characterization

The ultrasonic experiments were carried out by an ultrasonic disperser (BANDELIN sonorex digitec, 35 kHz, Germany). A Fourier transform infrared spectrometer (8101 M Shimadzu) was used in spectral studies of the tablet. The XRD patterns of the samples were collected on a Philips-PW1800 with Cu K $\alpha$  radiation ( $\lambda=1.54184\text{\AA}$ ) in the  $2\theta=4-90^\circ$  with steps of  $0.02^\circ$ , scanning operated at 40 kV and 30 mA (Netherlands). Field emission scanning electron microscopes (FESEM) were performed by Hitachi S-4160 model (Japan) to observe the surface morphologies of the nanoparticles. The electrical conductivity of compressed pellets of polymers and nanocomposites was measured using a standard four-probe set-up connected to a Keithley system comprising a voltmeter and a constant high-current source, made in IRAN.

## RESULTS AND DISCUSSION

### FTIR spectroscopy

Figure 1(a-c) shows FTIR spectra for a) B<sub>4</sub>C, b) TiO<sub>2</sub> and c) B<sub>4</sub>C/TiO<sub>2</sub>/PANI (50%wt). FTIR range of B<sub>4</sub>C has appeared in Figure 1a and no pinnacle is watched. Figure 1b delineates the infrared spectra of TiO<sub>2</sub>. The watched primary top at around 610 cm<sup>-1</sup> is ascribed to vibration extending methods of Ti-O. Figure 1c shows an FTIR range for B<sub>4</sub>C/TiO<sub>2</sub>/PANI (50%wt). The particular top around 1120 cm<sup>-1</sup> is related to vibrational methods of

N=Q=N (Q alludes to the quinonic type rings), demonstrating that PANI is shaped in our example. The tops at 1250 and 1110 cm<sup>-1</sup> are related to N-H bowing and hilter kilter C-N vibrational extending of the benzenoid rings, individually. The tops at 1480 and 1510 cm<sup>-1</sup> are ascribed to C=N and C=C extending of the PANI ring (like a benzoidal structure). Moreover, the wideband at 3400 cm<sup>-1</sup> compares to the symmetric extending vibration of O-H, N-H extending modes.

As indicated by the information referenced above, it is gathered that the asserted nanocomposite is effectively incorporated.

### XRD Data

Figures 2 and 3 show the example of XRD for B<sub>4</sub>C/TiO<sub>2</sub> and B<sub>4</sub>C/TiO<sub>2</sub>/PANI (50%wt) nanocomposites. The pinnacles displayed can be recorded as a rhombohedral grid of B<sub>4</sub>C. The determined cross-section constants are in acceptable understanding with the arranged qualities (JCPDS cards no. 00-035-0798, JCPDS cards no. 01-078-2486 for TiO<sub>2</sub>-1, JCPDS cards no. 01-072-1148 for TiO<sub>2</sub>-2, JCPDS cards no. 00-002-0406 for TiO<sub>2</sub>-3 and JCPDS cards no.01-075-2078 for graphite). By contrasting and the standard XRD design, the tops at  $2\theta=22, 24, 27, 44$  and  $2\theta=9.6, 12, 13, 53, 55$  are identified with B<sub>4</sub>C and B nanoparticles, separately (Kipcak et al., 2013). The boron carbide particles were not unadulterated boron carbide. As indicated by these Figures, TiO<sub>2</sub> nanoparticle shows three structures TiO<sub>2</sub>-1, TiO<sub>2</sub>-2 and TiO<sub>2</sub>-3 (anatase) and graphite shows the top at  $2\theta=26$ . The crystallite size decided from the FWHM of the fundamental impression of B<sub>4</sub>C and TiO<sub>2</sub> are 41 and around 31 nm, individually.

### SEM images

Figure 4(a-d) shows SEM images of a) B<sub>4</sub>C, b) TiO<sub>2</sub>, c) and d) B<sub>4</sub>C/TiO<sub>2</sub>/PANI nanocomposites with different scales. As shown in the figures, average size of B<sub>4</sub>C and TiO<sub>2</sub> are 46 and 31 nm. From the images, it can also be seen that all B<sub>4</sub>C and TiO<sub>2</sub> particles were coated by PANI, completely. Figures show clearly that the composites were fiber and cluster shaped. The average diameter fibers are 60-110 nm.

### Conductivity

Electrically conductivity of samples at room temperature was measured by four probe method. The conductivity of PANI after polymerization by APS as initiator and DBSA as dopant is 0.011 S/cm. When mass content of B<sub>4</sub>C

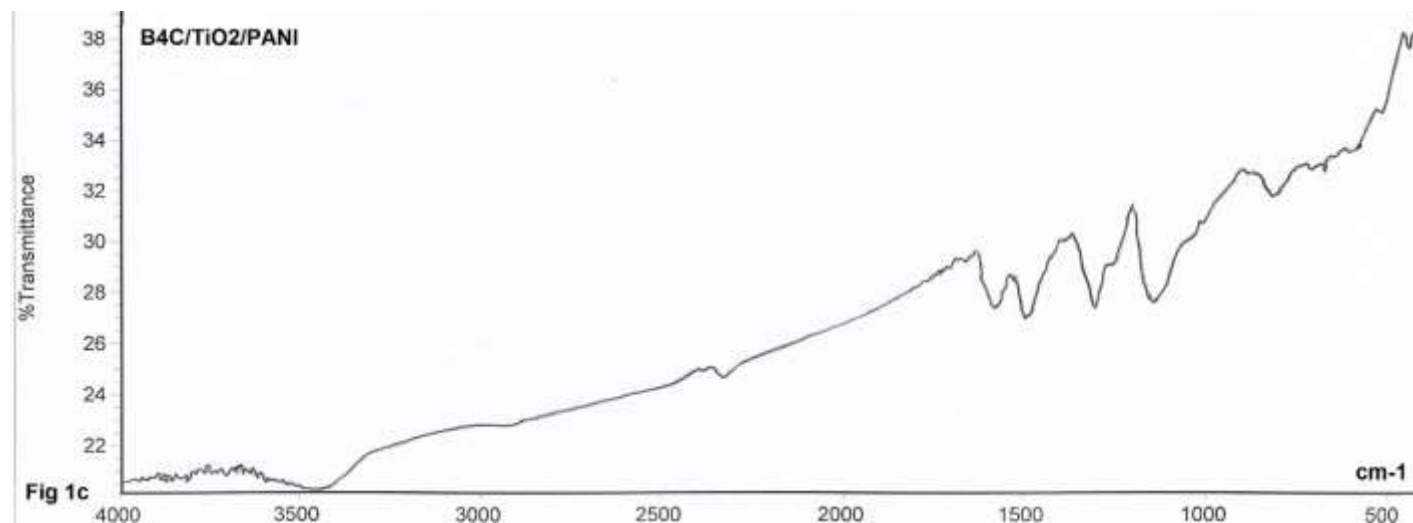
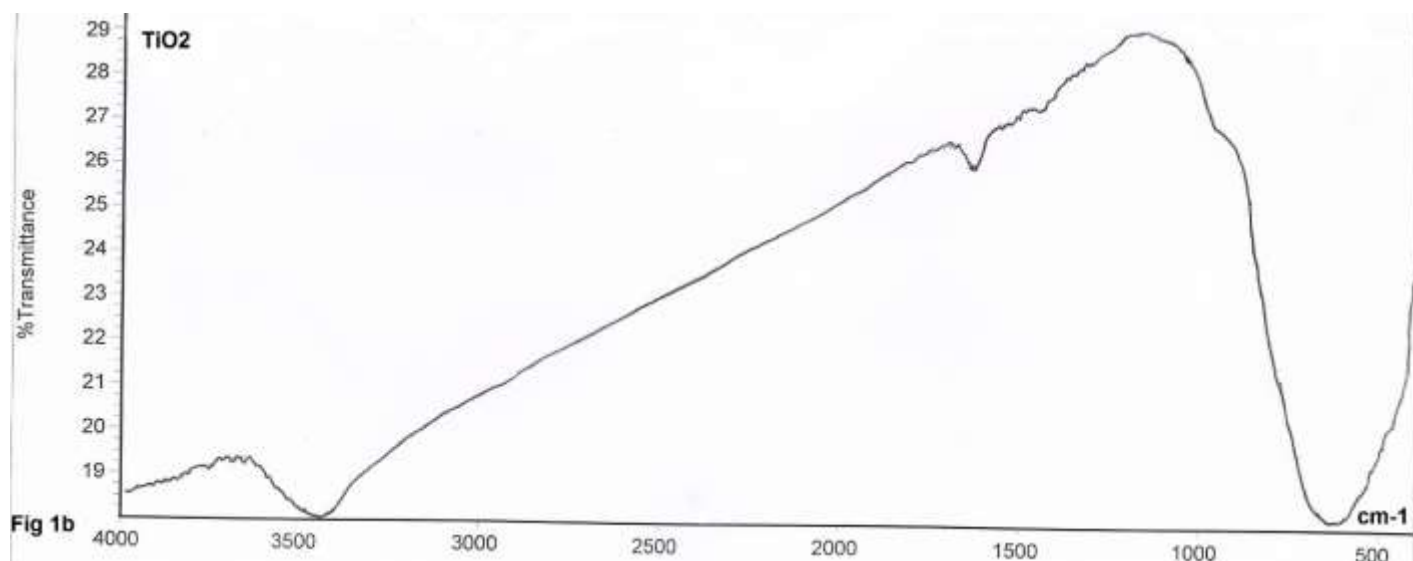
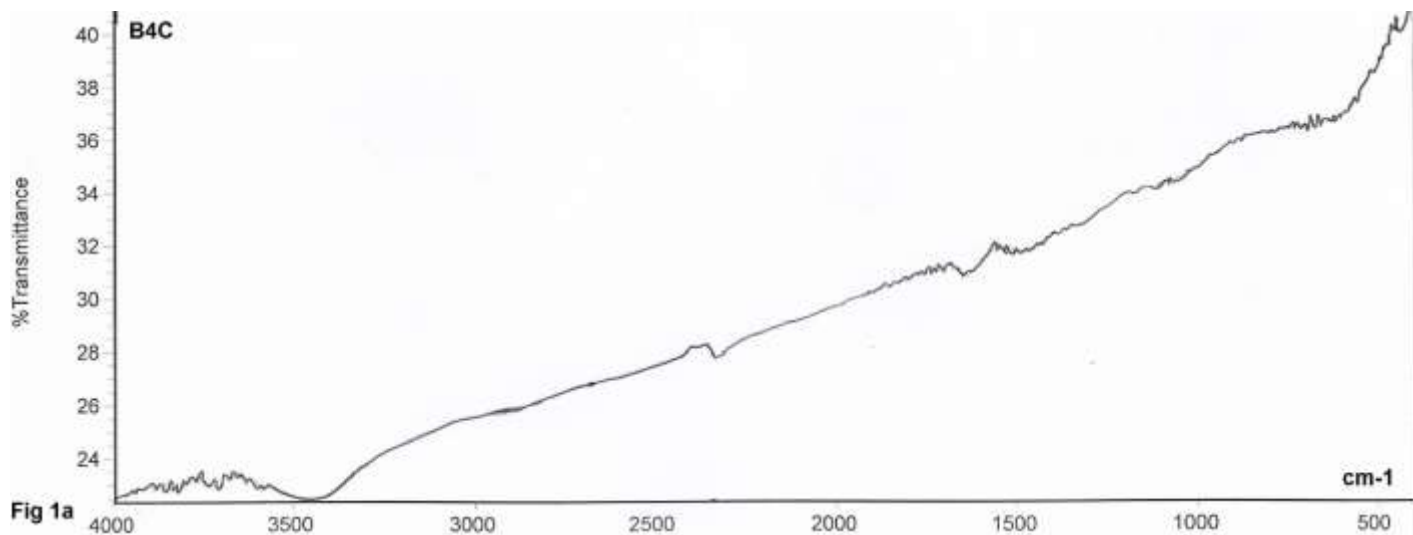


Figure 1. FT-IR spectra for a) B<sub>4</sub>C, b) TiO<sub>2</sub> and c) B<sub>4</sub>C/TiO<sub>2</sub>/PANI (50%wt).

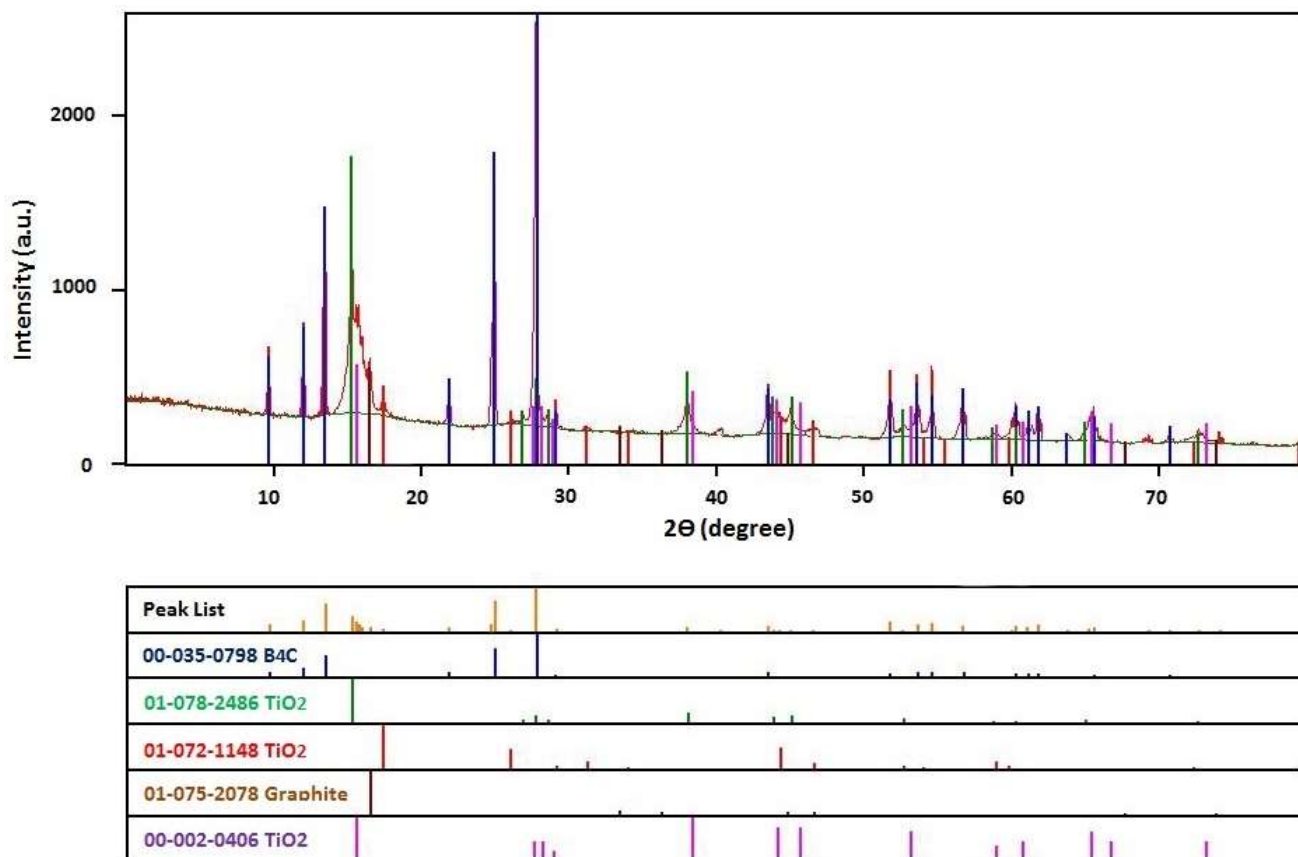


Figure 2. XRD pattern of B<sub>4</sub>C/TiO<sub>2</sub> nanoparticles.

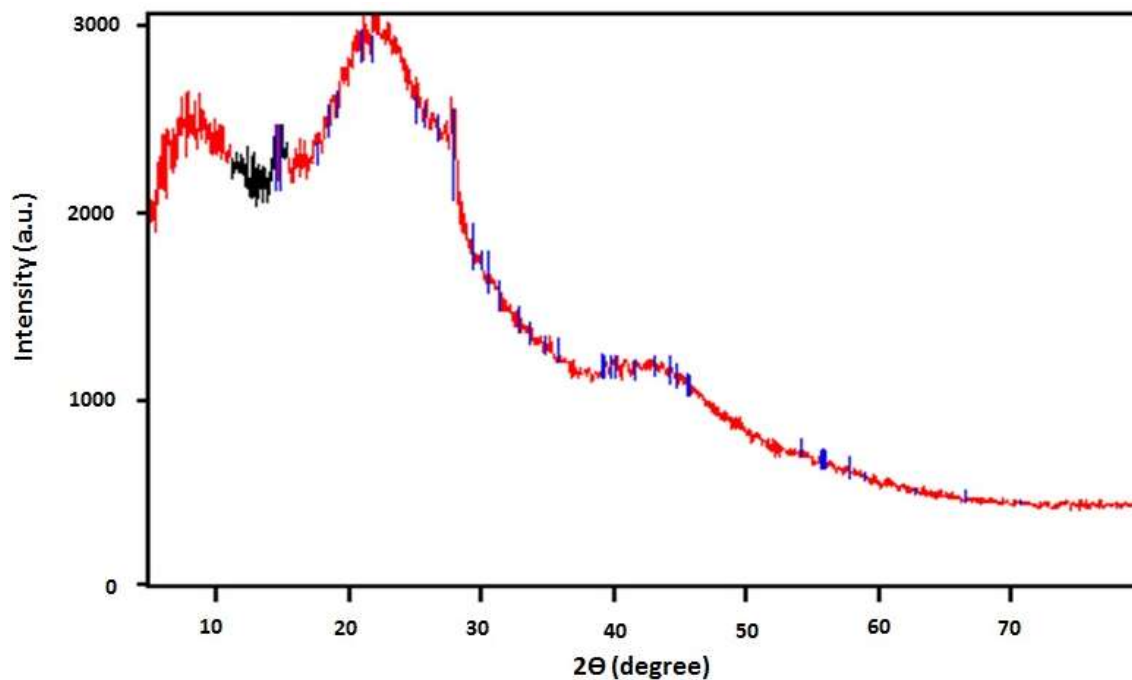


Figure 3. XRD pattern of B<sub>4</sub>C/TiO<sub>2</sub>/PANI (50%wt) nanocomposites.

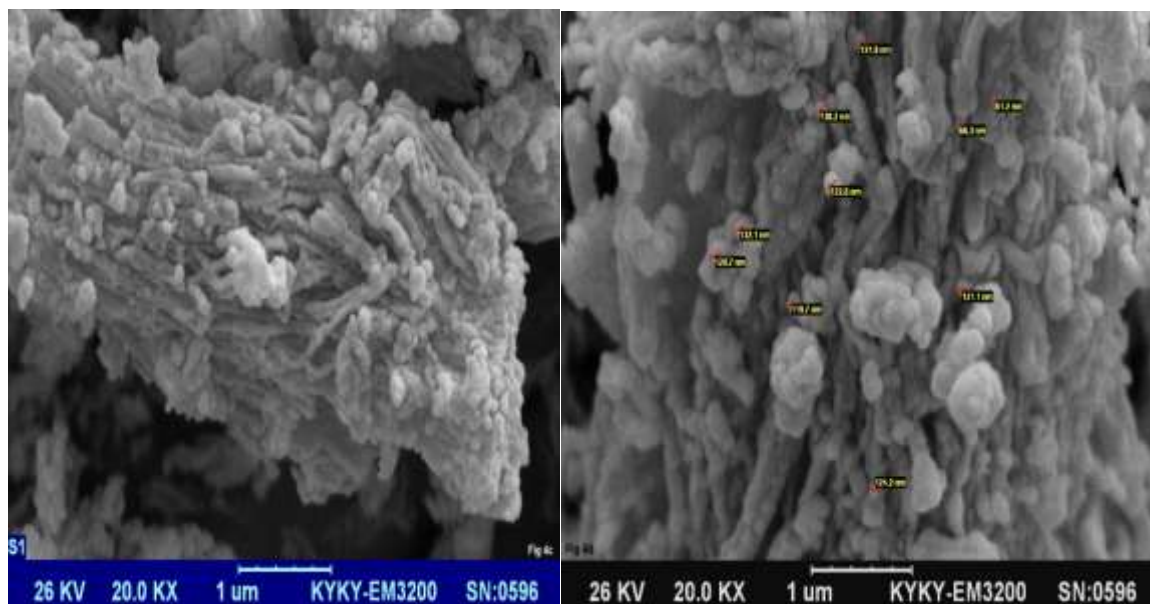


Figure 4. FE-SEM images of a) B<sub>4</sub>C, b) TiO<sub>2</sub>, c and d) B<sub>4</sub>C/TiO<sub>2</sub>/PANI nanocomposites with different scales.

**Table 1.** The electrical conductivity of B<sub>4</sub>C/TiO<sub>2</sub>/PANI nanocomposites.

Sample	Conductivity (S/cm)
PANI	0.011
B <sub>4</sub> C/TiO <sub>2</sub> /PANI 20wt%	6.1×10 <sup>-3</sup>
B <sub>4</sub> C/TiO <sub>2</sub> /PANI 50wt%	9.6×10 <sup>-4</sup>
B <sub>4</sub> C/TiO <sub>2</sub> /PANI 80wt%	2.5×10 <sup>-4</sup>

nanoparticles were incorporated, the conductivity of B<sub>4</sub>C/TiO<sub>2</sub>/PANI nanocomposites with different weight ratios was sharply reduced. Conductivities were decreased by increasing weight ratio of B<sub>4</sub>C as core. The decrease in conductivity of B<sub>4</sub>C/TiO<sub>2</sub>/PANI composites may be attributed to the insulating behavior of partial blockage of the conductive path. All conductivities are summarized in Table 1.

### Neutron shielding

The problem of efficient neutron shielding, in the environment of a spallation source, reduces to that of concentrating the largest possible quantity of boron atoms in the smallest possible volume, so as to obtain an efficient neutron absorbing material. Elemental boron is high price material; it is preferred to be used in boron-based compounds like, for example, boron carbide (B<sub>4</sub>C) or boron nitride (BN). The commercial price of B<sub>4</sub>C is lower than BN, so boron carbide plays a greater role in the industry as a neutron shield. For applications where more peculiar shapes are required, it is much more convenient to build a shielding object using a composite material where B<sub>4</sub>C represents a relevant portion of the composition (Celli et al., 2006). Here, an effective neutron shielding material is obtained by dissolving a different amount of B<sub>4</sub>C/TiO<sub>2</sub> powder into a PANI. The advantage of a composite material, for example a mixture made of B<sub>4</sub>C and TiO<sub>2</sub> with PANI, resides in the fact that the polymer matrix usually contains a large fraction of hydrogen atoms and its electrical conductivity. In fact, a solid mixture of boron carbide and TiO<sub>2</sub> powders with PANI represents one of the most diffuse shielding materials in a spallation neutron source facility.

### Theoretical methods for attenuation coefficients of neutron and gamma-rays

If a material of thickness, x is placed in the path of a beam of gamma radiations, the intensity of the beam will be attenuated according to the Beer–Lambert’s law,

$$I = I_0 e^{-\mu x} \tag{1}$$

where I<sub>0</sub> and I are the unattenuated and attenuated

photon intensities, respectively, and μ (cm<sup>-1</sup>) is the linear attenuation coefficient of the material.

The following relations represent half-value thickness (HVT, cm) in which the intensity of primary photon beam reduced by 1/2:

$$HVT = \ln 2 / \mu \tag{2}$$

A coefficient more accurately characterizing a given material is the density-independent mass attenuation coefficient μ/ρ (cm<sup>2</sup> g<sup>-1</sup>).

$$I = I_0 e^{-(\mu/\rho)\rho x} = I = I_0 e^{-(\mu/\rho)d} \tag{3}$$

where d is the mass per unit area (g cm<sup>-2</sup>). The mass attenuation coefficient, μ/ρ, for a compound or a mixture is given by

$$\mu/\rho = \sum_i w_i (\mu/\rho)_i \tag{4}$$

where ρ is the density of mass of the sample, and w<sub>i</sub> and (μ/ρ)<sub>i</sub> are the weight fraction and mass attenuation coefficient, respectively, of the constituent element j.

For a chemical compound, the fraction by weight is given by

$$w_i = \frac{a_i A_i}{\sum_j a_j A_j} \tag{5}$$

where A<sub>i</sub> is the atomic weight of the j<sup>th</sup> element and a<sub>i</sub> is the number of formula units. Hence the linear attenuation coefficients are given by:

$$\mu = \sum_i \rho_i (\mu/\rho)_i \tag{6}$$

where ρ<sub>i</sub> is the partial density, the density as it appears in the mixture, of j<sup>th</sup> constituent element. It is given by the product of the weight fraction of j<sup>th</sup> constituent w<sub>j</sub> and the density of the sample ρ as the following (Kaplan, 1989):

$$\rho_i = w_i \rho \tag{7}$$

For neutron attenuation calculations, the elastic and inelastic scattering reactions, and neutron-capture interaction process, are of great importance (Yilmaz et al., 2011).

Here, we used following equation:

$$Q = Q_0 e^{-\Sigma x} \tag{8}$$

where Q<sub>0</sub> and Q are the unattenuated and attenuated photon intensities, respectively, and Σ (cm<sup>-1</sup>) is the linear attenuation coefficient of the material.

The following relations represent half-value thickness (HVT, cm) in which the intensity of primary photon beam reduced by 1/2:

**Table 2.** Linear attenuation coefficient of thermal neutron for B<sub>4</sub>C/TiO<sub>2</sub>/PANI (20 wt% B<sub>4</sub>C) in various thicknesses.

Radionuclide	Material ID	E (eV)	d (mm)	$\varnothing_{(0)}$	$\varnothing$	$\ln(\varnothing/\varnothing_{(0)})$	$\Sigma$	$(\varnothing_{(0)}-\varnothing)\times 100/\varnothing_{(0)}$
<sup>252</sup> Cf	B <sub>4</sub> C/TiO <sub>2</sub> /PANI (20 wt% B <sub>4</sub> C)	0.025	1	7029	6295	0.11	11.03	10.44
		0.025	1.5	7029	5848	0.18	12.26	16.80
		0.025	2	7029	5685	0.21	10.61	19.12

**Table 3.** Linear attenuation coefficient of thermal neutron for B<sub>4</sub>C/TiO<sub>2</sub>/PANI (50 wt% B<sub>4</sub>C) in various thicknesses.

Radionuclide	Material ID	E (eV)	d (mm)	$\varnothing_{(0)}$	$\varnothing$	$\ln(\varnothing/\varnothing_{(0)})$	$\Sigma$	$(\varnothing_{(0)}-\varnothing)\times 100/\varnothing_{(0)}$
<sup>252</sup> Cf	B <sub>4</sub> C/TiO <sub>2</sub> /PANI (50 wt% B <sub>4</sub> C)	0.025	1	7029	4563	0.43	43.21	20.61
		0.025	1.5	7029	5018	0.34	22.46	28.61
		0.025	2	7029	5580	0.23	11.54	35.08

$$\text{HVT}=\ln 2/\Sigma \quad (9)$$

The attenuation coefficients of neutron ( $Q_0$  and  $Q$ ) of B<sub>4</sub>C/TiO<sub>2</sub>/PANI with different weight ratios and thickness were measured, without supplementary materials, at energy of 0.025 eV. The linear attenuation coefficients ( $\Sigma$ ), attenuation percentage ( $Q_0/Q \times 100$ ) and half-value thickness (HVT) have been measured and calculated via full width at half maximum (FWHM). Neutron attenuation calculations results with different weight ratios and thickness at 0.025 eV were summarized in Tables 2 to 4.

### Linear attenuation coefficient ( $\Sigma$ )

The higher the  $\Sigma$  value, the thermal neutron vitality goes through the material. Figure 5 portrays the information of the direct lessening coefficient comparative with neutron photon vitality (0.025 eV), for the B<sub>4</sub>C/TiO<sub>2</sub>/PANI nanocomposites with various weight proportions (20, 50 and 80wt% B<sub>4</sub>C) and thicknesses (1, 1.5 and 2 mm). It is seen that the readied nanocomposites have the most measure of lessening coefficient in the radionuclide source.

As appeared, for all examples with expanding weight proportions and thicknesses,  $\Sigma$  esteem has an exponential increment. The most elevated direct lessening coefficients were gotten for B<sub>4</sub>C/TiO<sub>2</sub>/PANI (80wt% B<sub>4</sub>C) and 1.5 and 2 mm thickness. In any case, B<sub>4</sub>C/TiO<sub>2</sub>/PANI 50wt% and 1 mm thickness is better. This coefficient relies upon the occurrence of photon vitality, the material thickness and the substance synthesis of materials. B<sub>4</sub>C and PANI are a potential competitor as a protecting material, accordingly, it is normal that an expansion in the substance of B<sub>4</sub>C nanoparticles, causes a compelling increment in the constriction coefficient esteem. Likewise utilizing

nanosized B<sub>4</sub>C would augment the connections of neutron-radiation and the nanocomposites adequately which brings about constriction of the photon. The acquired consequences of direct weakening coefficients of the examined nanocomposites appear in Tables 2 to 4.

### Thermal neutron attenuation percentage

The experimental measurement of attenuation percentage of B<sub>4</sub>C/PANI nanocomposites with different weight ratios and thicknesses are depicted in Figure 6. Attenuation percentage was increased by increasing weight ratios and thicknesses. It is observed that among the prepared samples, attenuation percentage was obtained at 0.025 eV. As observed, this trend is similar for all the samples within statistical errors. It is known that the attenuation percentage depends on the neutron energy and chemical composition of the compounds. Here, the higher concentration of B<sub>4</sub>C nanoparticles in the chemical composition of the nanocomposites, explains the greater capability in shielding thermal neutron. The most amount of neutron attenuation percentage is about 80%, which is observed for the sample of B<sub>4</sub>C/TiO<sub>2</sub>/PANI (80wt% B<sub>4</sub>C) in 2 mm. All obtained results of experimental measurement of attenuation percentage summarized are Tables 2 to 4.

### Half value thickness (HVT)

In this research, we also demonstrated the HVT, in some cases, characterize radiation shielding properties directly. The concept of HVT is used to quantify the ability of a neutron beam to penetrate the material being examined. The variation of values of HVT for the prepared samples is given in Figure 7. The HVT is the thickness of a

**Table 4.** Linear attenuation coefficient of thermal neutron for B<sub>4</sub>C/TiO<sub>2</sub>/PANI (80 wt% B<sub>4</sub>C) in various thicknesses.

Radionuclide	Material ID	E (eV)	d (mm)	$\varnothing_{(0)}$	$\varnothing$	$\ln(\varnothing/\varnothing_{(0)})$	$\Sigma$	$(\varnothing_{(0)}-\varnothing) \times 100/\varnothing_{(0)}$
<sup>252</sup> Cf	B <sub>4</sub> C/TiO <sub>2</sub> /PANI (80 wt% B <sub>4</sub> C)	0.025	1	7029	4787	0.38	38.41	31.89
		0.025	1.5	7029	4534	0.44	29.23	35.49
		0.025	2	7029	4439	0.46	22.98	36.84

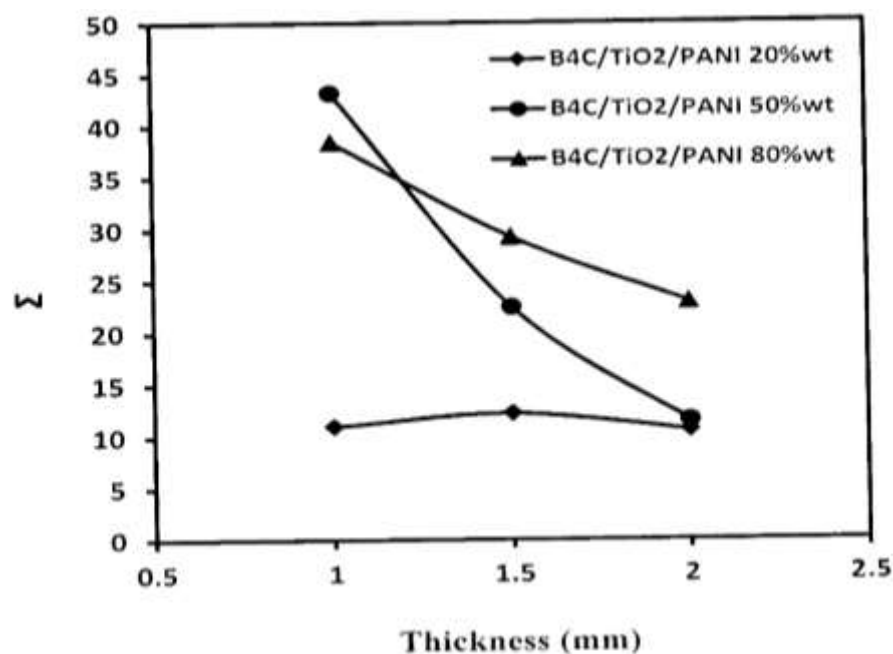


**Figure 5.** The linear attenuation coefficient of B<sub>4</sub>C/TiO<sub>2</sub>/PANI nanocomposites in different weight ratios (20, 50 and 80wt% B<sub>4</sub>C) and thicknesses at 0.025 eV.

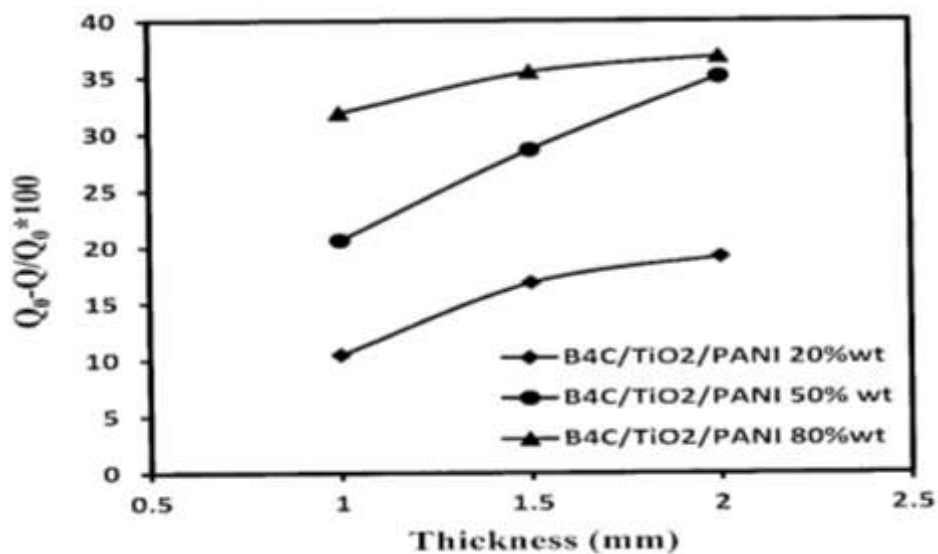


**Figure 6.** The variation of attenuation percentage of B<sub>4</sub>C/TiO<sub>2</sub>/PANI nanocomposites in different weight ratios (20, 50 and 80wt% B<sub>4</sub>C) and thicknesses at 0.025 eV.

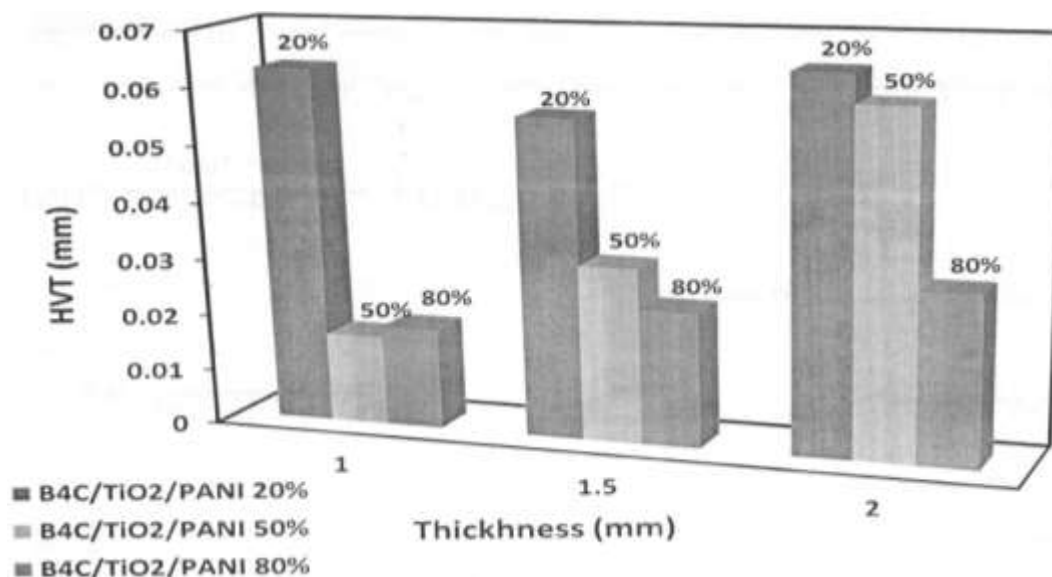


Figure 7. Comparison of shielding thickness in term of half value thickness at different energies.

homogeneous absorber that attenuates the narrow beam intensity to one-half of the original intensity. For a better radiation shielding material, a low value of HVT parameter is desired. The HVT inversely proportional to the attenuation coefficient of photons will result in the increasing of target sample HVT.

## Conclusion

Neutron shielding absorbers using  $B_4C/TiO_2/PANI$  was fabricated for testing, and the characteristics for neutron transmission and neutron-shielding were experimentally evaluated. The  $B_4C$  was shown to be practical and as effective as the other available shielding absorber using a conducting polymer for fabrication and industry applications such as PANI. The results provide confirming data that  $B_4C/TiO_2/PANI$  can be easily synthesized and it is an excellent candidate to be used as a usual organic solvent and water insoluble neutron absorber.  $TiO_2$  helps to gain better processability and having more composite of  $B_4C$  in PANI, too.

## CONFLICT OF INTERESTS

The authors have not declared any conflict of interests.

## REFERENCES

Azooz MA, El-Batal FH (2009). Gamma ray interaction with transition metals-doped lead silicate glasses. *Materials Chemistry and Physics* 117:59-65.

- Bartali L, Becherini F, Grazi F, Zoppi M (2009). Surface scattering efficiency of some common materials for shielding pulsed neutron scattering instruments. *Nuclear Instruments and Methods in Physics Research Sect A* 608:360-362.
- Celli M, Grazi F, Zoppi M (2006). A new ceramic material for shielding pulsed neutron scattering instruments. *Nuclear Instruments and Methods in Physics Research A* 565:861-863.
- Chen C, Wang L, Liu X, Yang W, Lin J, Chen G, Yang X (2019).  $K_0.5Na_0.5NbO_3-SrTiO_3/PVDF$  Polymer Composite Film with Low Remnant Polarization and High Discharge Energy Storage Density. *Polymers* 11: 310-321.
- D'Mellow B, Thomas DJ, Joyce MJ, Kolkowski P, Roberts NJ, Monk SD (2007). The replacement of cadmium as a thermal neutron filter. *Nuclear Instruments and Methods in Physics Research A* 577:690-695.
- Dolabi MB, Azimi A, Hosseini SH (2019). Preparation of thermal infrared and microwave absorber using  $WO_3/MnFe_3O_4$ /polyaniline nanocomposites. *Materials Research Innovations* (<https://doi.org/10.1080/14328917.2019.1677078>, In press).
- Fugaru V, Bercea S, Cristian P, Gheorghe M (2015). Gamma Ray Shielding Properties of Some Concrete Materials. *Acta Physica Polonica Series A* 127(4):1427-1429.
- Hosseini SH, Zamani P, Mousavi SY (2015a). Thermal infrared and microwave absorbing properties of  $SrTiO_3/SrFe_{12}O_{19}$ /polyaniline nanocomposites. *Journal of Alloys and Compounds* 644:423-429.
- Hosseini SH, Alamian A, Mousavi SM (2016). Preparation of magnetic and conductive graphite nanoflakes/ $SrFe_{12}O_{19}$ /polythiophene nanofiber-nanocomposites and its radar absorbing application. *Fibers and Polymers* 17:593-599.
- Hosseini SH, Asadnia A, Moloudi M (2015b). Preparation and electromagnetic wave absorption hard-soft Ba ferrite/polypyrrole core-shell nanocomposites. *Materials Research Innovations* 19(2):107-112.
- Hosseini SH, Ezzati SN, Askari M (2015c). Synthesis, characterization and X-ray shielding properties of polypyrrole/lead nanocomposites. *Polymers for Advanced Technologies* 26:561-568.
- Hosseini SH, Soltanabadi Z (2016). Investigation of X-ray shielding properties of Au nano-composite-based polyaniline. *Material Research Innovations* 20:300-306.
- Hosseini SH, Zamani P (2016). Preparation of thermal infrared and microwave absorber using  $SrTiO_3/BaFe_{12}O_{19}$ /polyaniline

- nanocomposites. *Journal of Magnetism and Magnetic Materials* 397:205-212.
- Hosseini SH, Azimi A, Dolabi MB (2019). Study of UV-Visible and near infrared absorption CsXWO<sub>3</sub>/polypyrrole nanocomposite. *Materials Research Innovations* (online; <https://doi.org/10.1080/14328917.2019.1677302>).
- Hu P, Ji, Z, Shen Z, Wan P, Liu X (2018) High dielectric constant and energy density induced by the tunable TiO<sub>2</sub> interfacial buffer layer in PVDF nanocomposite contained with core-shell structured TiO<sub>2</sub>@BaTiO<sub>3</sub> nanoparticles. *Applied Surface Science* 441:824-831.
- Kaplan MF (1989). *Concrete Radiation Shielding*. John Wiley & Sons, Inc., New York.
- Kim SC, Cho SH (2019). Analysis of the Correlation between Shielding Material Blending Characteristics and Porosity for Radiation Shielding Films. *Applied Sciences* 9(9):1765.
- Kipcak AS, Gurses P, Derun EM, Tugrul N, Piskin S (2013). Characterization of boron carbide particles and its shielding behavior against neutron radiation. *Energy Conversion and Management* 72:39-44.
- Modal S, Banthia AK (2005). Low-temperature synthetic route for boron carbide. *Journal of the European Ceramic Society* 25:287-291.
- Nambiar S, Yeow JT (2012). Polymer-Composite Materials for Radiation Protection, *ACS Applied Materials and Interfaces* 4(11):5717-5726.
- Onimus F, Bechade JL, Gilbon D (2013). Experimental Analysis of Slip Systems Activation in Neutron-Irradiated Zirconium Alloys and Comparison with Polycrystalline Model Simulations. *Metallurgical and Materials Transactions A* 44A:S45-S60.
- Sukegawa AM, Aanyama Y, Ohnishi S, Sakurai S, Kaminaga A, Okuno K (2011). Development of Flexible Neutron-Shielding Resin as an Additional Shielding Material. *Journal of Nuclear Science and technology* 48:585-590.
- Wozniak AI, Ivanov VS, Zhdanovich OA, Nazarov VI, Yegorov AS (2017). Modern Approaches to Polymer Materials Protecting from Ionizing Radiation. *Oriental Journal of Chemistry* 33(5):2148-2163.
- Yılmaz E, Baltas H, Kırıs E, Ustabas I, Cevik U, El-Khayatt AM (2011). Gamma ray and neutron shielding properties of some concrete materials. *Annals of Nuclear Energy* 38:2204-2212.
- Yiping H, Weijiang Z, Lu L, Jiao X, Zhou C (2013). A "Sandwich" type of neutron shielding composite filled with boron carbide reinforced by carbon fiber. *Chemical Engineering Journal* 220:143-150.
- Zhang P, Li Y, Wang W, Gao Z, Wang B (2013). The design, fabrication and properties of B<sub>4</sub>C/Al neutron absorbers. *Journal of Nuclear Materials* 437:350-358.